Composite Structures 153 (2016) 442–450

Contents lists available at ScienceDirect

Composite Structures

journal homepage: www.elsevier.com/locate/compstruct

Detection and characterisation of delamination damage propagation in Woven Glass Fibre Reinforced Polymer Composite using thermoelastic response mapping

Ayad Kakei [a,b], J.A. Epaarachchi [a,*], Mainul Islam [a], J. Leng [d,e], N. Rajic [c]

[a] Centre of Excellence in Engineered Fibre Composites, University of Southern Queensland, West Street, Toowoomba, QLD 4350, Australia
[b] University of Kirkuk, College of Engineering, Kirkuk, Iraq
[c] Defence Science & Technology Group, 506 Lorimer Street, Fishermans Bend, VIC 3207, Australia
[d] School of Mechanical & Electrical Engineering & Centre of Excellence in Engineered Fibre Composites, University of Southern Queensland, West Street, Toowoomba, QLD 4350, Australia
[e] Centre for Smart Materials and Structures, School of Astronautics, Harbin Institute of Technology, Harbin 150001, China

ARTICLE INFO

Article history:
Received 9 January 2016
Revised 2 June 2016
Accepted 20 June 2016
Available online 22 June 2016

Keywords:
Delamination
Thermoelastic Stress Analysis
Cohesive element
Local bending

ABSTRACT

This paper details a study on the application of Thermoelastic Stress Analysis (TSA) for the investigation of delamination damage propagation in glass fibre reinforced composite materials. A woven Glass (0/90)/Epoxy composite sample containing a purposely created delamination was subjected to a step-cyclic loading (varying mean level) whilst monitoring the thermoelastic response of the sample with an infrared camera. A finite element analysis (FEA) was performed using cohesive elements to simulate the propagation of the delamination under a monotonically increasing axial load. It is shown that the delamination crack length inferred from the TSA results is consistent with microscopic analysis of the sample, and that the measured crack growth rate is in reasonable agreement with simulation results.

1. Introduction

Glass Fibre reinforced polymer (GFRP) composite has been used in many critical engineering applications due to its superior strength to weight ratio. However, despite its use over many decades, there remain many unresolved problems relating to internal damage initiation and propagation in GFRP materials. An in-depth knowledge of the strength and damage tolerance capabilities of GFRP is of course an essential input to the design process for structural load-bearing applications. Unfortunately, the complex nature of the damage accumulation process in GFRP materials is not yet completely understood. This is one of the reasons for the limited use of GFRP in aerospace applications.

Delamination between plies is one of the critical failure modes of GFRP because it significantly reduces inter-laminar strength. The growth of a delamination leads to a rapid decline in the mechanical properties of GFRP which has the potential to cause catastrophic failure [24,26]. This has led to considerable research on the subject. Although theoretical modelling has yielded valuable insights into the delamination process (e.g. [15,16,20,22,27,35], none of the developed models have been shown to accurately predict the delamination process for the full range of GFRP materials. More work on model development is needed.

Many non-destructive techniques have been developed over past decades for the detection of delamination in composites. Acoustic emission [28], ultrasonics [14], shearography [33], thermography [5,8,9,11] are some of the major established technologies. The primary attraction of thermographic techniques is that they furnish full-field imagery and thereby are generally much more rapid than point-wise alternatives such as conventional ultrasonics and tap testing. A number of different variants have been successfully applied to composite inspection, including pulsed thermography [18], lock-in thermography [13] and sonic thermography [17,21]. Whilst Thermoelastic Stress Analysis (TSA) is seldom categorised as a non-destructive inspection tool it has the capacity to be used in that role quite effectively. Indeed, in providing a proxy measurement of bulk stress it can offer insights into the structural significance of damage, something that few other NDI techniques are able to provide. Recent studies have shown that TSA is a potentially powerful investigative tool for structural damage in fibre reinforced polymeric materials. For example, Haj-Ali & Elhajjar [8] used TSA to study damage in a single lap joint using TSA and correlated their measurements to microstructural analysis

* Corresponding author.
E-mail address: eparracj@usq.edu.au (J.A. Epaarachchi).

http://dx.doi.org/10.1016/j.compstruct.2016.06.044
0263-8223/

of the specimen. This study demonstrated that TSA was able to identify the early stages of damage in bonded joints. However, the investigation of delamination by TSA remains a relatively narrow research field and more studies are warranted on a wider range of FRP materials.

Digital image correlation (DIC), another optical full-field technique, has also been applied to the study of damage in composite materials. DIC provides a measurement of surface deformation which can be converted to an estimate of strain by computing the appropriate spatial derivatives [1]. It has been successfully applied to investigate the initiation and propagation of damage in composite materials [6]. Although DIC has some advantages over TSA, e.g. a capacity to be applied under static loading conditions and historically lower equipment costs, in practice it yields a lower effective stress sensitivity and is generally difficult to apply to complex-shaped (i.e. non-planar) structural components.

The high capital-cost disadvantage of TSA no longer applies following a recent finding that low-cost automation grade thermal detectors can provide comparable stress sensitivities to cryogenically cooled photon detectors [23,25]. Thermal detectors are generally far less expensive, much smaller, have better tolerance to shock and vibration and consume less power than their photon-detector counterparts. This has brought about increased opportunities for the industrial and research utilisation of TSA.

2. Thermoelastic Stress Analysis (TSA)

TSA is a full field stress measurement technique based on the thermoelastic effect [7]. Thermoelasticity describes a phenomenon by which a solid changes its temperature when subject to a volume change caused by external loading. The thermoelastic effect was given a theoretical foundation by William Thomson (Lord Kelvin) in 1853, who demonstrated [34] a linear relationship between the temperature change in a solid and the change in the sum of principal stresses:

$$\frac{\Delta T}{T_0} = -K_0 \Delta\sigma, \tag{1}$$

where T_0 is the absolute temperature of the solid, $K_0(=\lambda/\rho Cp)$ is the thermoelastic constant, λ is the linear thermal expansion coefficient, ρ the mass density, Cp the specific heat at constant pressure, and $\Delta\sigma = \Delta(\sigma_1 + \sigma_2 + \sigma_3)$ is the change in the first stress invariant.

This equation, formulated for a homogeneous isotropic solid, can be extended to orthotropic materials [32]

$$\rho C_p \frac{\Delta T}{T_0} = -(\alpha_{11}\Delta\sigma_{11} + \alpha_{22}\Delta\sigma_{22}) \tag{2}$$

where α_{nn} is the coefficient of thermal expansion. In order to apply Eqs. (1) and (2) to stress measurement one requires a measurement of very small surface temperature variations, of the order of milli-Kelvin. Traditionally, such measurements have relied on the use of cryogenically cooled photon detectors, largely because of the superior dynamic response and noise equivalent temperature sensitivity of this class of radiometer. However, in the present study, measurements are made using a lower cost automation-grade microbolometer, a class of thermal detector that previous work has shown can yield stress sensitivities that are comparable to vastly more expensive photon detectors.

3. Finite element simulation of crack surface

Delamination in composite materials has been widely investigated numerically over many decades. Considering the complex nature of most delamination problems, the finite element method (FEM) is found to be the most suitable tool for simulation. The Virtual Crack Closure Technique (VCCT) has been utilised in the investigation of delamination in many published studies [12,30]. VCCT analysis relies upon two basic hypotheses; namely, that the energy released during crack growth is identical to the energy required to close the crack and the stress state does not change significantly

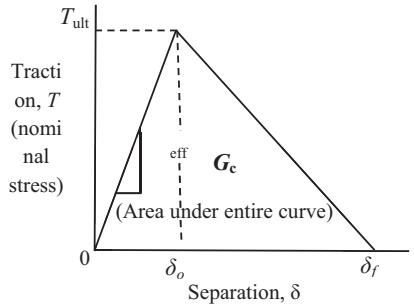

Fig. 1. Cohesive parameters of typical bilinear traction-separation model [4].

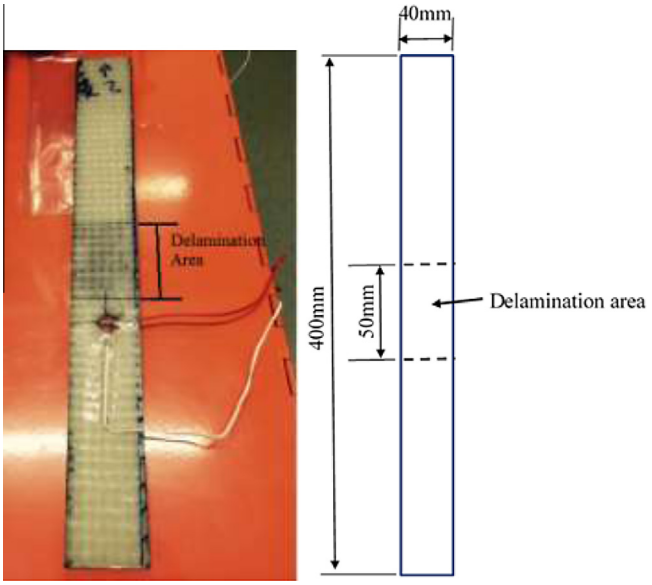

Fig. 2. Glass/Epoxy specimen (400 mm × 40 mm × 7.5 mm).

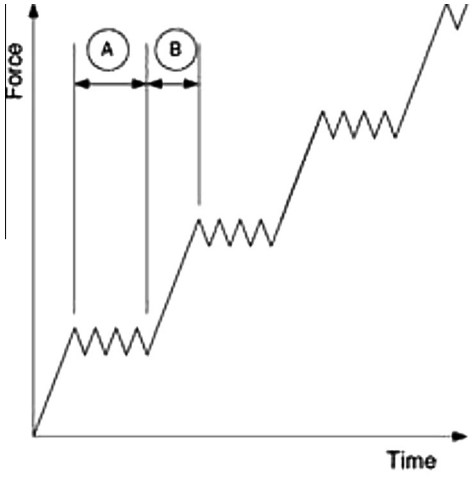

Fig. 3. TSA test method, a static load step is applied, followed by a cyclic loading about this mean loading level [11].

when the crack is extended [3]. These hypotheses significantly influence the accuracy of the VCCT analysis as they explicitly ignore plasticity in the analysis [12]. In addition, another major drawback of the VCCT method is that it requires a priori knowledge of the initial crack size [31]. An alternative to VCCT is the Cohesive Zone Method (CZM) which is becoming more popular in the analysis of delamination in composite materials, largely because of its simplicity and usability [36]. CZM has been used in many studies into the simulation of delamination crack propagation in composite materials. A probabilistic CZM was developed by Shanmugam et al. [29] to capture steady-state energy release rate variations in Double Cantilever Beam (DCB) delamination specimens. Wang and Xu [36] presented an approach using cohesive elements to simulate propagation of a delamination, including descriptions of both propagation direction and effective propagation length under high-cycle fatigue loading. Saeedifar et al. [28] and Haselbach et al. [10] have shown that the modified CZM technique exhibits good performance in simulating crack initiation and delamination crack length in laminated composite structures.

The cohesive approach is based on the concept of the cohesive crack model. This concept was developed by Barenblatt [2] who introduced cohesive forces in order to solve the equilibrium problem in elastic bodies with cracks. The cohesive damage zone models relate tractions to displacement jumps at an interface when a crack occurs. As shown in Fig. 1, the area under the traction-displacement curve is equal to the fracture toughness G_C.

The aim of the present work is to use TSA and finite element analysis (using cohesive elements) to develop an improved understanding of the propagation of delamination under quasi-static and dynamic loading. The role of local bending at the crack tip of a delamination is also investigated.

4. Experimental procedure

4.1. Materials and specimen geometry

The material examined in the present work is a fifteen-layer (0/90) AR 145 E-glass woven roving (398 g/m^2 weight and 0.5 mm thickness) fibre-reinforced epoxy resin matrix composite that has a nominal density of 1698 kg/m^3. Woven roving fabric is an appropriate glass material for hand lay applications where uni-

Fig. 4. Thermo-elastic stress analysis (TSA) testing setup.

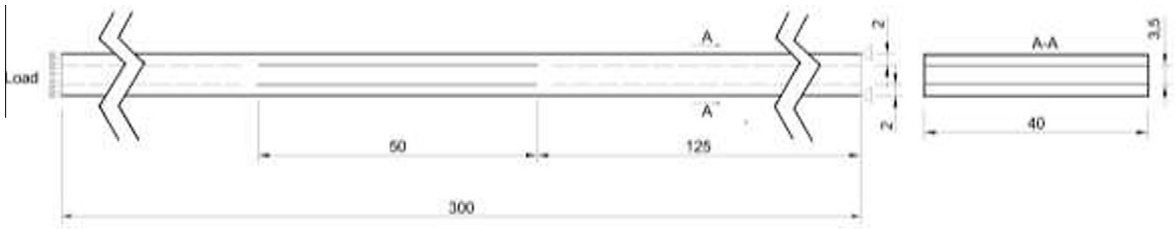

Fig. 5. Model Geometry (dimensions are in millimetres).

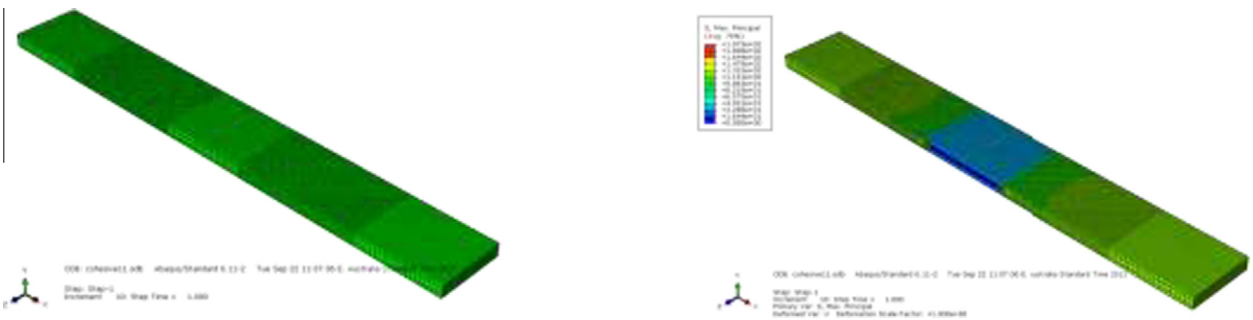

Fig. 6. Three dimensional finite element model of the delaminated specimen.

form thickness and transverse strength is required. The woven roving fabric offers good coverage, drape-ability, and fast wet-out. Kenetix R246TX epoxy resin was used as the matrix material. The plain weave structure of the WC laminate consisted of two mutually orthogonal directions (warp and weft) with an approximate glass volume fraction of 60%. Two artificial delaminations 50×40 mm^2 in size were made between the 4th–5th and 11th–12th layers respectively (relative to the bottom), by embedding Teflon paper (0.001 mm thickness) during manufacture. One large specimen was manufactured and then cut into smaller rectangular 400×40 mm^2 coupons as shown in Fig. 2. Each coupon was coated with aerosol matt black paint to produce a uniformly high surface emissivity for thermographic inspection.

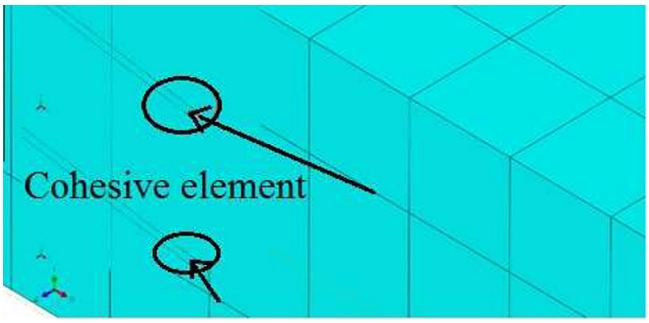

Fig. 7. Cohesive elements.

Table 1
Mechanical and damage behaviours for Woven Glass Fibre Reinforced Polymer Composite.

Material properties	Cohesive properties		
	Critical energy release rate G_{Cn} (mJ)	Cohesive damage stress behaviour (MPa)	Stiffness (MPa/mm)
$E_1 = E_2 = 15{,}000$ MPa $E_3 = 9500$ (MPa) $G_{12} = G_{13} = 6527.53$ (MPa) $G_{23} = 7000$ MPa $\nu_{12} = \nu_{13} = 0.126$ $\nu_{23} = 0.263$	$G_{CI} = 0.4146$ $G_{CII} = 1.0525$	$t_n = 5$ $t_t = t_s = 15$	$K_{nn} = 9500$ $K_{ss} = 6527.53$

4.2. Mechanical testing

The samples were tested using a constant amplitude cyclic load which was applied around a mean load that was increased incrementally from 5 kN to 35 kN in steps of 5 kN (Fig. 3). Each increase in mean load was applied under displacement control at a rate of 1.5 mm/min. The cyclic-load amplitude was 3 kN and approximately 10000 cycles were applied at each step at a frequency of 5 Hz. All tests were conducted in an MTS 810 100 kN uniaxial testing machine fitted with hydraulic grips. The specimen was fastened into the machine with approximately 50 mm of specimen gripped at each end. Load and displacement measurements were acquired from load cell and displacement sensors. Electrical resistance foil strain-gauges were attached to the sample surface and were used to measure the strains during the applied loading. This strain gauge signal also served as a reference for the TSA.

As the cyclic loading imparts relatively little strain energy to the delamination area, the effects of fatigue were not considered in the present analysis [11] .

The schematic of the TSA setup is shown in Fig. 4. The TSA system used a FLIR A325 commercial microbolometer camera. This device contains a 320 (H) $\times$ 240 (V) Vanadium Oxide (VOx) array with a noise equivalent temperature detectivity (NETD) of 50 mK. The camera outputs data in 16-bit digital form supplied at a fixed rate of 60 frames per second.

4.3. Cohesive zone model

A finite element model of the aforementioned specimen was created in Abaqus 6.13 and used to predict mixed-mode multi-delamination growth. Cohesive elements or double nodes are used to represent the bonded interfaces. The specimen geometry and loading regime are depicted in Fig. 5. The layered specimen dimensions are 300 mm long, 7.5 mm thick (15 layers) and 40 mm wide, loaded at one end in the longitudinal direction and fixed at the other end. The model includes two initial delamination cracks. Both initial cracks are 50 mm in length and are located 125 mm from the end of the specimen. The first crack is located 1.75 mm below the mid-plane of the specimen, whilst the second crack is located symmetrically 1.75 mm above the mid-plane. The distance between the two initial cracks is 3.5 mm.

The specimen was modelled using 3D solid elements (C3D8I) with the top and bottom parts of the specimen (referring to the

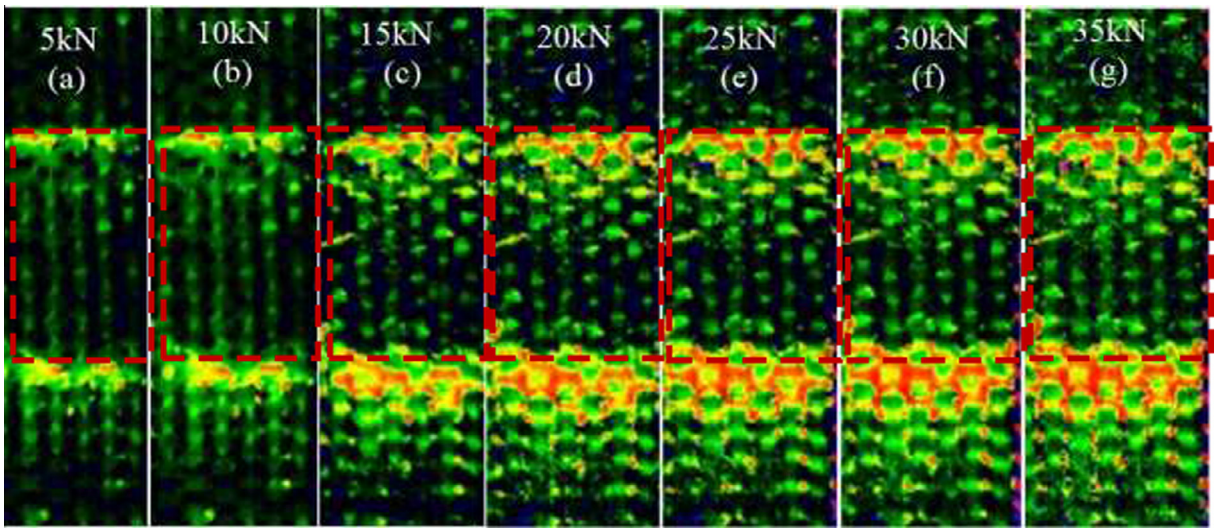

Fig. 8. Delamination crack front propagation (θ-component). Red dotted line outlines the boundary of the initial delamination. Delamination zone is seen to increase as a function of mean load.

sections above and below the cracks) consisting of 8 layers (a thickness of 4 mm), and the middle section 6 layers (a thickness of 3.5 mm). Each part was separately meshed using different mesh sizing. The finite element model is shown in Fig. 6. Two debonded interfaces were defined, one between the 4th and 5th layers and the other between the 11th and 12th layers, consistent with the actual delamination (see Fig. 7). Delamination growth was simulated using cohesive elements (COH3D8) 0.001 mm in thickness embedded at the interfaces. The user cohesive elements technique was implemented by means of inputting a user material subroutine UMAT. Auto Desk© Simulation composite analysis 2015 Plug-ins© for Abaqus 6.13 were used to create the UMAT subroutine to calculate the nine state variables for the cohesive materials [36]. These state variables are stored by Abaqus at each individual integration point within the finite element model. They were represented in the Abaqus/viewer application by the solution-dependent state variables "SDVN" where N is the unique integer which identifies the state variable (SDV1, SDV2,. . ., SDV9). The nine state variables are defined as follows: SDV1 represents the current damage state, SDV2 is a continuous real variable between zero and one which indicates the damage initiation criterion has been satisfied, SDV3 is the effective traction at damage initiation, SDV4 is the effective displacement at damage initiation, SDV5 is the maximum effective displacement attained in the loading history, SDV6 is the damage variable D, a continuous real variable which varies between zero and one, SDV7 is the work done in the normal loading mode (local 3-direction), SDV8 is the work done in the first shear loading mode (local 1-direction), and SDV9 is the work done in the second shear loading mode (local 2-direction). The cohesive elements in the model act as a "traction-separation" element type. Cohesive elements (COH3D8) with properties defined by UMAT were inserted between the specimen parts within the connected area. The influence of the COH3D8 elements on the model as a whole can be ignored as softening of the element was not taken into consideration. Simulation related material properties are detailed in Table 1. All mechanical and cohesive properties were determined experimentally according to ASTM standards in the Centre of Excellence in Engineering Fibre Composite Laboratories at the University of Southern Queensland. Mode I cohesive properties were obtained according to ASTM D5528-13 and Mode II cohesive properties were obtained according to ASTMD7905-14.

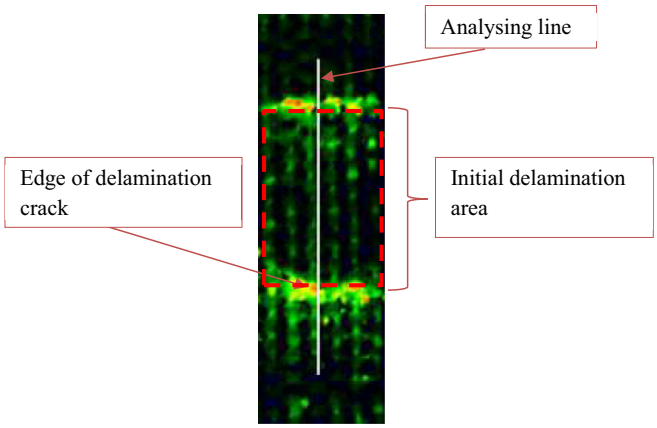

Fig. 9. Analysis line used in estimating the delamination crack length.

4.4. Microscopic investigation

Before final failure, the specimen was removed from the MTS testing machine and investigated using a microscope. The specimen was cut along the axial direction using a water jet cutter. The cutting direction was determined from the TSA data obtained during testing. The cut edges of the sectioned pieces were polished. High pressure air was used to remove any remaining dust on the specimen. The sectioned specimen was observed under OLYMPUS XC10 and OLYMPUS BX41M microscopes and images were captured and saved for post-processing. Measurements of the crack location obtained from microscopic examination were compared to estimates determined from TSA.

5. Results and discussion

Fig. 8 shows the thermoelastic phase response of the sample measured during cyclic loading of the sample. The variations in

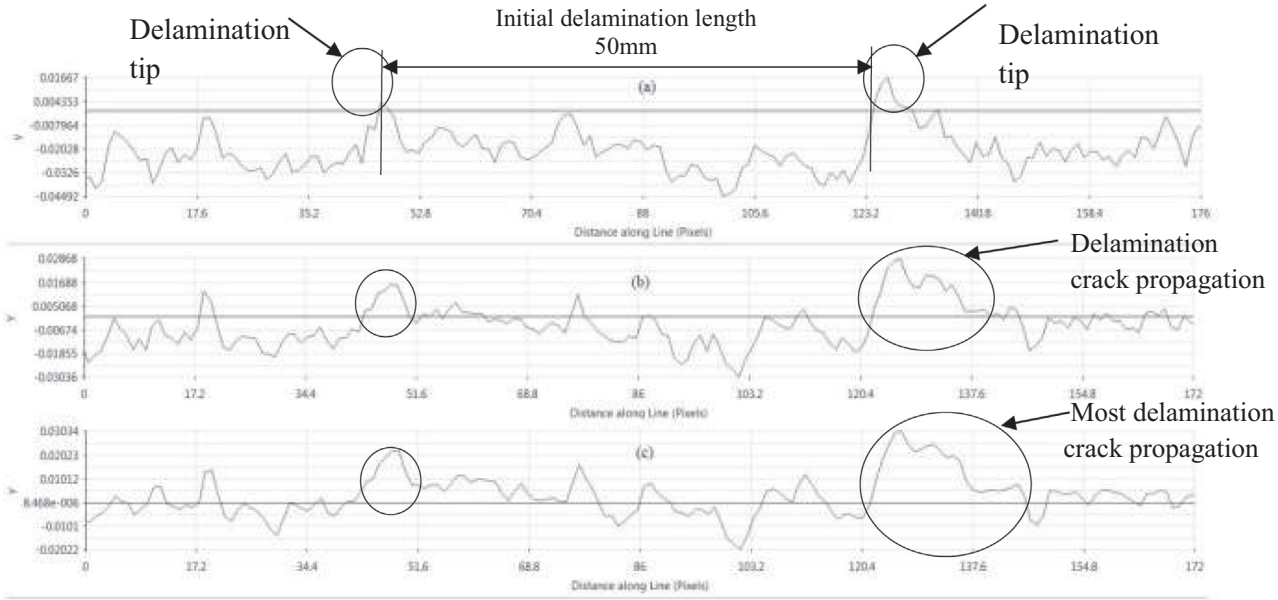

Fig. 10. Quadrature signal (Y) in the delamination region at mean loads of. (a) 5 kN (0.11% max strain), (b) 20 kN (0.44 % max strain) and (c) 35 kN (0.78% max strain) with propagating delamination crack. The vertical axis is in Kelvin (nom.), and the horizontal axis corresponds to distance in pixels (50 mm = 76.7 pixels).

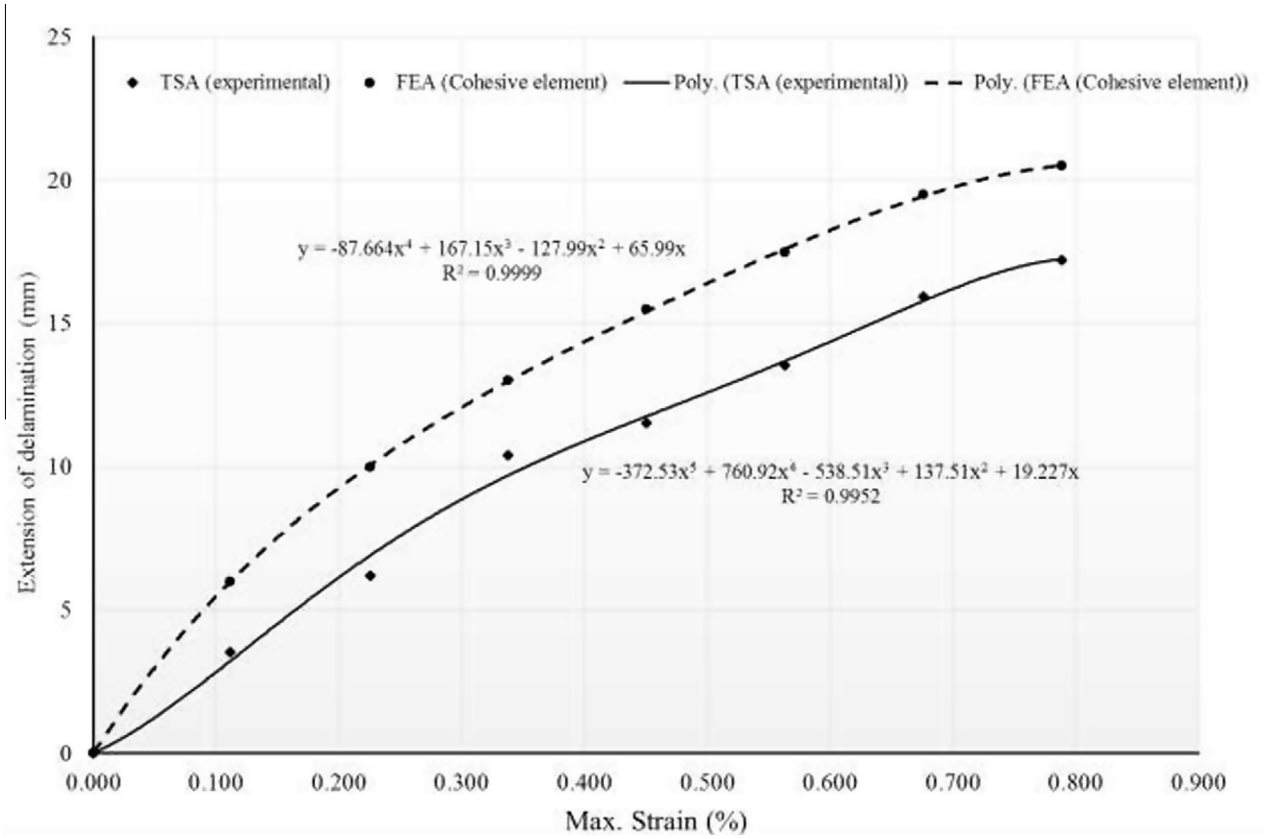

Fig. 11. Average extension delamination length-Max. Strain % of woven glass fibre reinforced polymer [0/90] specimen under different loadings corresponding with delamination crack propagation in Fig. 11.

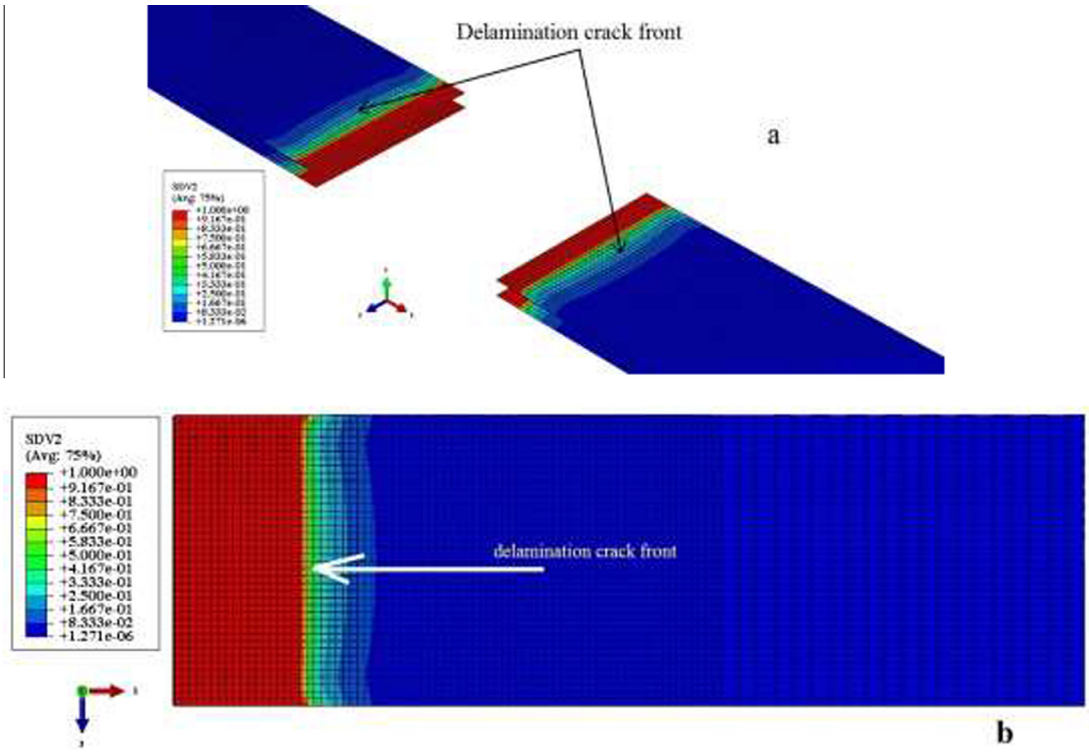

Fig. 12. Plot of the damage variable SDV2, (a) damage in the cohesive elements (full model) at 5 kN (0.111% strain), (b) damage in the cohesive element in one of the cohesive sections at 25 kN (0.563 % strain).

colour correspond to variation in the phase of the thermoelastic response relative to the load, with the largest variations in phase occurring near the bottom edge of the delamination zone. The original size of the delamination is approximately shown by the red dotted line in frame (a) to (g). This is seen to correspond reasonably well with an area of perturbed phase response (defined by red hues) at the lowest mean load of 5 kN (0.11% strain). As the mean load is increased this area grows, and reaches a maximum at the final mean load of 35 kN (0.77 % strain).

The quadrature component of the thermoelastic response signal, which is driven by heat conduction and therefore quite sensitive to stress gradients, was examined along the centre line of the specimen through the delamination as shown in Fig. 9. Fig. 10 shows the signal magnitude along this line for load cases (a), (d) and (g) in Fig. 8. The tip of the delamination is seen to correspond to an increasingly positive quadrature signal. The magnitude of this signal and the area it envelops increases with increasing mean load.

An estimate of the delamination crack length was extracted from the quadrature signal by measuring the distance between the extremities of the peaks circled in Fig. 10. These estimates are presented in Fig. 11. The delamination grows monotonically with increasing load, as expected, however the rate is seen to decline. This is possibly a result of an increasing number of local cracks in the composite sample. The agreement between the experimental and numerical results is generally good in terms of the overall trend, but the latter yields consistently higher estimates for the delamination length. The fact there is a difference is not surprising as the peak value in the measured quadrature response is not necessarily coincident with the position of the delamination crack front, though as Fig. 11 confirms there is a reasonable correlation. Further modelling work is underway to develop a deeper understanding of the relationship between the two.

ABAQUS solution dependent state variables, SDV2 and SDV6, are displayed in Figs. 12 and 13 respectively. State variable SDV2 represents the failure index at each integration point. It is a continuous variable that can have a value between 0 and 1. A value of 0 indicates there are no stresses at the integration point. A value of 1 indicates that the failure initiation criterion has been satisfied and the process of damage evolution (stiffness reduction) has begun at the integration point. Another useful state variable is SDV6, which is referred to as the damage variable D. SDV6 is a continuous variable with a value between 0 and 1 where a value of 0 corresponds to an undamaged integration point that has its original (full) stiffness, and a value of 1 corresponds to a fully degraded (zero stiffness) integration point.

The primary failure mechanism was thought to be a combination of Mode I and Mode II damage at the delamination crack front caused by local bending. This was investigated using a cohesive element model in Abaqus 6.13 software. Fig. 14 shows the normal

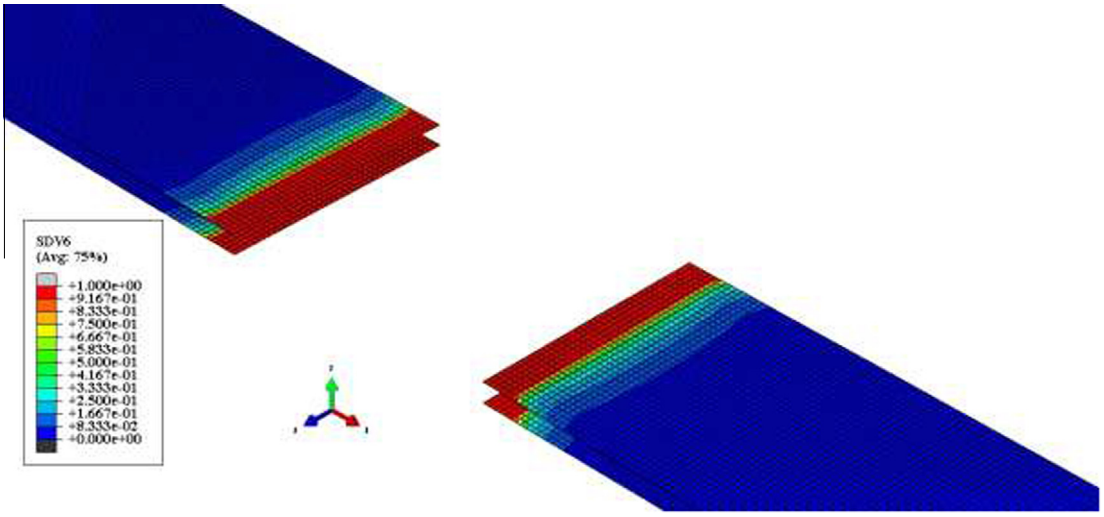

Fig. 13. Plot of the damage variable SDV6.

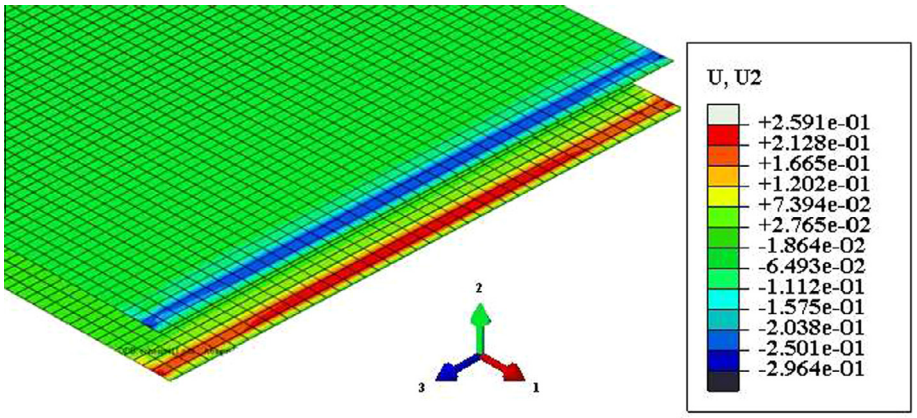

Fig. 14. Deformation mode in thickness direction (2) indicates significant local bending in front of delamination crack.

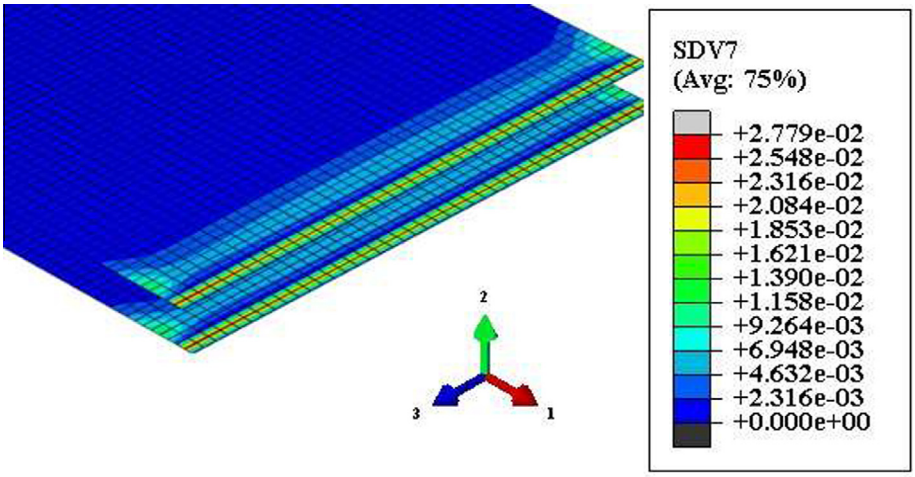

Fig. 15. SDV7 state variable for cohesive elements (local bending) in front of delamination crack.

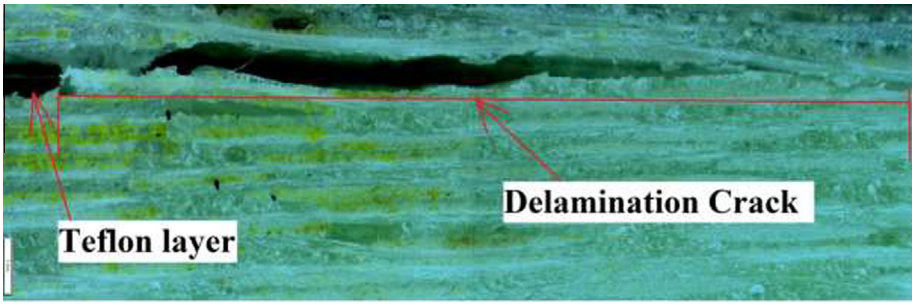

Fig. 16. Photograph showing a 16.34 mm delamination crack extending from a Teflon insert, after loading to 35 kN.

displacement in the cohesive elements in front of the delamination crack at an applied load of 35kN. The displacement pattern is consistent with local bending which supports the proposed failure mechanism. The delamination crack propagation has caused a reduction in the bending stiffness. Multicontinuum Theory (MCT) state variable 'SDV7' was deployed to investigate the local bending phenomenon. For woven composites SDV7 stores the material temperature for longitudinal cracking in the fill-matrix constituent used for hysteresis heating computations. Fig. 15 shows the simulated delamination crack propagation and provide an accurate insight to the local bending phenomenon.

To corroborate the information obtained from TSA the specimen was investigated under an optical microscope. Fig. 16 shows a detailed micrograph of the delamination crack in the specimen following completion of the last step in the loading sequence to a peak value of 35 kN. Based on a visual determination of the crack tip location the crack length was estimated at 16.34 mm. This is consistent with the value determined by TSA, which as shown in Fig. 11 is approximately 17 mm. Although the two values are remarkably close one should recall that assigning the peak quadrature response as an estimate for the crack tip location was done on a somewhat arbitrary basis. Further study is required to understand the relationship between this particular metric and the physical location of the crack tip. On another cautionary note, the strongly heterogeneous response evident in Fig. 8, which is due to the woven structure of the laminate, leads to a position dependency in the estimate derived for the crack tip, an effect that was not considered in the present work. This also requires further study.

6. Conclusion

The delamination damage growth of a $[0/90]_{15}$ Woven Glass Fibre Reinforced Polymer Composite has been investigated experimentally and numerically. A monotonically increasing quasi-static load and a step-cyclic load regime have been applied to a specimen with a purposely created delamination and its thermoelastic response measured using a microbolometer. Subsequently, a microscopic analysis was performed on the damaged area of the specimen. The delamination crack length was measured and compared with numerical results.

A measurable change in the thermoelastic response indicated the development of a delamination crack between layers at a relatively low applied strain. By contrast, there was no evident increase in delamination crack length in the final load increment from 30 to 35 kN, indicating that the specimen had already reached its fracture point load.

An analysis of the delamination process in ABAQUS 6.13 has revealed that a cohesive element model provides reasonable accuracy for the simulation of damage growth in the class of specimen considered. It was shown that local bending in front of the delamination crack tip is the primary cause for propagation of the delamination, suggesting that both Mode I and II failure are important under quasi-static and fatigue loading.

Acknowledgements

The authors thank Mr. Mohan Trada for his assistance and help in sample testing and the microscopic investigation.

References

[1] Pan B, Qian KM, Xie HM, Asundi A. Two-dimensional digital image correlation for in-plane displacement and strain measurement: a review. Meas Sci Technol 2009;20(6):062001.

[2] Barenblatt G. The mathematical theory of equilibrium cracks in brittle fracture. Adv Appl Mech 1962;7:55–129.

[3] Bonhomme J, Argüelles A, Viña J, Viña I. Numerical and experimental validation of computational models for mode I composite fracture failure. Comput Mater Sci 2009;45(4):993–8.

[4] Chen D, El-Hacha R. Cohesive fracture study of a bonded coarse silica sand aggregate bond interface subjected to mixed-mode bending conditions. Polym Polym Compos 2014;6:12–38.

[5] Colombo C, Vergani L. Influence of delamination on fatigue properties of a fibreglass composite. Compos Struct 2014;107:325–33.

[6] Crupi V, Guglielmino E, Risitano G, Tavilla F. Experimental analyses of SFRP material under static and fatigue loading by means of thermographic and DIC techniques. Compos B Eng 2015;77:268–77.

[7] Thermoelastic stress analysis. In: Greene R, Patterson E, Rowlands R, editors. Springer handbook of experimental solid mechanics. USA: Springer; 2008.

[8] Haj-Ali R, Elhajjar R. An infrared thermoelastic stress analysis investigation of single lap shear joints in continuous and woven carbon/fiber epoxy composites. Int J Adhes Adhes 2014;48:210–6.

[9] Haj-Ali R, Wei B-S, Johnson S, El-Hajjar R. Thermoelastic and infrared-thermography methods for surface strains in cracked orthotropic composite materials. Eng Fract Mech 2008;75(1):58–75.

[10] Haselbach PU, Bitsche RD, Branner K. The effect of delaminations on local buckling in wind turbine blades. Renewable Energy 2016;85:295–305.

[11] Johnson S. Thermoelastic stress analysis for detecting and characterizing static damage initiation in composite lap shear joints. Compos B Eng 2014;56:740–8.

[12] Jokinen J, Wallin M, Saarela O. Applicability of VCCT in mode I loading of yielding adhesively bonded joints—a case study. Int J Adhes Adhes 2015;62:85–91.

[13] Junyan L, Yang L, Fei W, Yang W. Study on probability of detection (POD) determination using lock-in thermography for nondestructive inspection (NDI) of CFRP composite materials. Infrared Phys Technol 2015;71:448–56.

[14] Karabutov AA, Podymova NB. Quantitative analysis of the influence of voids and delaminations on acoustic attenuation in CFRP composites by the laser-ultrasonic spectroscopy method. Compos B Eng 2014;56:238–44.

[15] Kashtalyan M, Soutis C. The effect of delaminations induced by transverse cracks and splits on stiffness properties of composite laminates. Compos A Appl Sci Manuf 2000;31(2):107–19.

[16] Keshava Kumar S, Ganguli R, Harursampath D. Partial delamination modeling in composite beams using a finite element method. Finite Elem Anal Des 2013;76:1–12.

[17] Kuhn E, Valot E, Herve P. A comparison between thermosonics and thermography for delamination detection in polymer matrix laminates. Compos Struct 2012;94(3):1155–64.

[18] Liang T, Ren W, Tian GY, Elradi M, Gao Y. Low energy impact damage detection in CFRP using eddy current pulsed thermography. Compos Struct 2016;143:352–61.

[20] Liu PF, Islam MM. A nonlinear cohesive model for mixed-mode delamination of composite laminates. Compos Struct 2013;106:47–56.

[21] Meola C, Boccardi S, Carlomagno GM, Boffa ND, Monaco E, Ricci F. Nondestructive evaluation of carbon fibre reinforced composites with infrared thermography and ultrasonics. Compos Struct 2015;134:845–53.

[22] Nair A, Roy S. Modeling of permeation and damage in graphite/epoxy laminates for cryogenic tanks in the presence of delaminations and stitch cracks. Compos Sci Technol 2007;67(11–12):2592–605.

[23] Rajic Nick, Rowlands D. Thermoelastic stress analysis with a compact low-cost microbolometer system. Quant InfraRed Thermogr J 2013;10:135–58.

[24] O'Brien TK. Characterization of delamination onset and growth in a composite laminate. In: Reifsnider KL, editor. *Damage in composite materials*, ASTM STP 775. USA: Am. Sot. Testing Marter; 1982. p. 140–67.

[25] Rajic N, Weinberg S, R D. Low-cost thermoelastic stress analysis. Mater Aust J Multi-Disciplinary Eng 2007;20(4):40–1.

[26] Talreja Ramesh, Singh CV. Damage and failure of composite materials, Cambridge, Unuited Kingdom, 2012.

[27] Rebière JL, Gamby D. A decomposition of the strain energy release rate associated with the initiation of transverse cracking, longitudinal cracking and delamination in cross-ply laminates. Compos Struct 2008;84(2):186–97.

[28] Saeedifar M, Fotouhi M, Ahmadi Najafabadi M, Hosseini Toudeshky H. Prediction of delamination growth in laminated composites using acoustic emission and Cohesive Zone Modeling techniques. Compos Struct 2015;124:120–7.

[29] Shanmugam V, Penmetsa R, Tuegel E, Clay S. Stochastic modeling of delamination growth in unidirectional composite DCB specimens using cohesive zone models. Compos Struct 2013;102:38–60.

[30] Shokrieh MM, Rajabpour-Shirazi H, Heidari-Rarani M, Haghpanahi M. Simulation of mode I delamination propagation in multidirectional composites with R-curve effects using VCCT method. Comput Mater Sci 2012;65:66–73.

[31] Shor O, Vaziri R. Adaptive insertion of cohesive elements for simulation of delamination in laminated composite materials. Eng Fract Mech 2015;146:121–38.

[32] Stanely P, Chan WK. The application of thermoelastic stress analysis techniques to composite materials. J Strain Anal Eng Des 1988;23 (3):137–42.

[33] Taillade F, Quiertant M, Benzarti K, Aubagnac C. 20 – Non-destructive evaluation (NDE) of composites: using shearography to detect bond defects A2. In: Karbhari Vistasp M, editor. Non-Destructive Evaluation (NDE) of Polymer Matrix Composites. Woodhead Publishing; 2013. pp. 542–57e.

[34] Thomson W. On dynamical theory of heat. Trans R Soc Edinburgh 1853;20:261–83.

[35] van der Meer FP, Moës N, Sluys LJ. A level set model for delamination – Modeling crack growth without cohesive zone or stress singularity. Eng Fract Mech 2012;79:191–212.

[36] Wang C, Xu X. Cohesive element analysis of fatigue delamination propagation in composite materials with improved crack tip tracking algorism. Compos Struct 2015;134:176–84.